Solid State Science and Technology, Vol. 34, No. 1 (2026) 1-10
https://doi.org/10.66514/ssst34-1-1-10

Impedance Studies of Heterogeneous BSCF-Ni-based Cathode Material at Intermediate Temperatures

*Nurulhuda Ahyad[1], Suhaida Dila Safia[2], Chung-Jen Tseng[3], Nafisah Osman[2,4], Abdul Mutalib Md Jani[1,4]**

[1]Faculty of Applied Sciences, Universiti Teknologi MARA, 35400 Tapah Road, Tapah, Perak, Malaysia

[2]Faculty of Applied Sciences, Universiti Teknologi MARA, 02600 Arau, Perlis, Malaysia

[3]Center for Energy Research, National Central University, No.300, Zhongda Rd., Zhongli, District, Taoyuan City 320317, Taiwan

[4]Proton Ceramic Fuel Cells Research Group, Faculty of Applied Sciences, Universiti Teknologi MARA, 40450 Shah Alam, Malaysia

**Corresponding author (email: abdmutalib@uitm.edu.my)*

(Received: 8 March 2026 / Revised: 6 May 2026 / Accepted: 11 May 2026 / Published online: 12 May 2026)

ABSTRACT

Intermediate-temperature solid oxide fuel cells (IT-SOFCs) offer a promising route to high-efficiency, low-emission energy conversion. However, the development of highly efficient IT-SOFCs is limited by the performance of their key components, particularly the cathode, for instance, $Ba_{0.5}Sr_{0.5}Co_{0.8}Fe_{0.2}O_{3-\delta}$ (BSCF). Although the BSCF exhibits high oxygen-ion and electronic conductivity, it suffers from phase instability and thermal expansion mismatch. To overcome limitations and enhance material performance, this study focuses on incorporating nickel (Ni) into BCSF to form heterogeneous BSCF-Ni composites. Experimental studies demonstrate that a single cell using heterogeneous BSCF-Ni cathodes achieves a polarization resistance as low as 10.80 Ω cm², compared to 22.32 Ω cm² for homogeneous BSCF-Ni at 750 °C. DRT peaks have shown that the heterogeneous BSCF-Ni enhances oxygen reduction and reduces polarization resistance, thereby improving overall cell performance. These advancements confirm that BSCF-Ni composites, enabled by doping and nanostructuring strategies, are highly promising cathode materials for durable, efficient IT-SOFC systems.

Keywords: heterogeneous BSCF-Ni, nanotubes, anode-supported single cell

INTRODUCTION

In recent years, the development of intermediate-temperature solid oxide fuel cells (IT-SOFCs) has emerged as a promising solution for efficient and sustainable energy

conversion [1,2]. Among various reported cathode materials (2-6), $Ba_{0.5}Sr_{0.5}Co_{0.8}Fe_{0.2}O_{3-\delta}$ (BSCF) has attracted significant attention for its excellent electrical conductivity and oxygen reduction reaction (ORR) activity at intermediate temperatures (600-800 °C) [3]. However, challenges such as cathode degradation and performance instability persist, hindering their practical application [4,5,6].

Nickel (Ni)-based materials are recognized for their high catalytic activity and electrical conductivity, making Ni a potential candidate for cathode modification to enhance electrochemical performance. The addition of nickel to a BSCF cathode (Ni-BSCF) [7] and the implementation of an electrode nanotube structure [8] are strategic methods to address the challenges faced by pure BSCF cathode materials. Ni is added to enhance the high oxygen diffusivity of BSCF by incorporating Ni's electronic properties, potentially overcoming the limitations of pure BSCF cathodes [7]. Furthermore, the heterogeneous structure of BSCF (a mixture of nanospherical and nanotube powders) has been reported to exhibit higher electrochemical performance than homogeneous nanospherical BSCF [8,9]. Although there is a previous study on heterostructure BSCF-Ni, it involved only phase heterostructure through surface reconstruction and conventional mixed microstructures. In contrast, this study focuses on the morphological heterostructure formed by combining nanotubes with a nanospherical structure. Despite progress, the performance of heterogeneous Ni-BSCF in the intermediate-temperature range remains poorly documented, highlighting a research gap.

Basically, in the electrochemical impedance studies, the impedance data are analyzed by a complex non-linear least squares (CNLS) fitting using an equivalent circuit model (ECM). The Voigt circuit is employed as a model of impedance spectra, in which impedance is expressed as a combination of circuit components such as capacitors, resistors, and inductors [10]. However, its efficacy is hindered by inherent limitations, including challenges in discerning between anode and cathode impedance responses [11]. Other than that, relying solely on CNLS fitting to extract the actual electrochemical responses of the depressed impedance arcs can lead to a misleading interpretation [12]. Another approach to analyzing and interpreting depressed arcs more comprehensively is via distribution relaxation time (DRT). Each electrochemical process can be effectively differentiated by its unique relaxation time. Therefore, DRT analysis is currently gaining increasing interest [13,14,15].

This study aims to investigate the electrochemical performance of a heterogeneous BSCF-Ni cathode and provide valuable insights into its behavior compared to homogeneous BSCF-Ni. The influence of microstructural heterogeneity on cathodic oxygen reduction kinetics is systematically evaluated under intermediate-temperature SOFC operating conditions. Electrochemical impedance spectroscopy is analyzed using both complex non-linear least-squares fitting based on an equivalent circuit model and relaxation-time distribution analysis to decouple overlapping electrochemical processes. Particular emphasis is placed on resolving cathode-related contributions and identifying the dominant rate-limiting steps in oxygen surface exchange, charge transfer, and diffusion. By correlating impedance features with relaxation-time distributions, this work seeks to a clearer structure–performance relationship and to demonstrate the effectiveness of heterogeneous Ni–BSCF cathodes for enhanced IT-SOFC performance.

MATERIALS AND METHODS

Powder synthesis and single-cell fabrication

In a nutshell, the respective NiO-$BaCe_{0.54}Zr_{0.36}Y_{0.1}O_{3-\delta}$ (BCZY) anode and BCZY electrolyte were prepared by the sol-gel method as previously reported [16,17]. To this solution, complexing agents such as EDTA, citric acid, and ethylene glycol were added, and the mixture was stirred until a homogeneous solution was obtained. The mixture underwent several drying and heating steps, including calcination, to obtain a single-phase precursor powder for BCZY and NiO-BCZY. The single-phase electrolyte and anode powders were produced at a calcination temperature of 1100 for BCZY and 1100 for NiO-BCZY.

The preparation of the cathode material involved several steps. Initially, the homogeneous $Ba_{0.5}Sr_{0.5}Co_{0.7}Fe_{0.2}Ni_{0.1}O_{3-\delta}$ (BSCF-Ni) powder was synthesized by a combined EDTA-citric acid complexing sol-gel method. Analytically pure reagents $Ba(NO_3)_2$, $Sr(NO_3)_2$, $Co(NO_3)_2{\cdot}6H_2O$, $Fe(NO_3)_3{\cdot}9H_2O$ and $Ni(NO_3)_2{\cdot}6H_2O$ (all from ACROS) were weighed with a stoichiometric ratio and dissolved in deionized water to form a homogeneous solution. Ethylenediaminetetraacetic acid (EDTA) and citric acid (CA), served as complexing agents, were added into the solution and the pH of the solution was adjusted to 6. A transparent gel was obtained after continuous heating and stirring. This gel was then heated in an air oven at 150 °C for 15 h, yielding a black solid precursor. The precursor was calcined in air at 900 °C for 5 h to form fine BSCF-Ni powder. Secondly, the nanoporous anodic aluminum oxide (NAAO) template was prepared through a two-step electrochemical anodization process, followed by sol-gel template synthesis via spin coating, as outlined in [8,9]. Then, the NAAO templates were fully dissolved in 0.5 M NaOH solution for 2 hours to get free individual BSCF nanotubes. The nanotube suspension was thoroughly washed with deionized water until the suspension reached pH 7 using pH indicator strips. Finally, the transition to a heterogeneous structure by mixing as-prepared BSCF-Ni nanotubes with BSCF-Ni powder at a ratio of 10 wt. % : 90 wt. %, respectively. The resulting heterogeneous BSCF-Ni ($BSCF\text{-}Ni_{10NTs:90NPs}$) was then subjected to careful sonication under degas mode at 30℃ for 2 minutes, followed by overnight drying in an oven at 80 °C.

An anode-supported single cell was then fabricated using the as-prepared powders. A 25 mm diameter, and 1.2 mm thick anode support pellet was manufactured using a dry pressing method at a pressure of 9 tones for 7 min. After the sintering process, the anode support was then layered with the prepared electrolyte using a spin-coating method and sintered at 1450 °C for 5 h, followed by the cathode layers. The cell configuration of NiO-BCZY|BCZY| heterogeneous BSCF-Ni was then treated at 900 °C for 2 h to produce a complete single cell, which was labeled as shown in Figure 1.

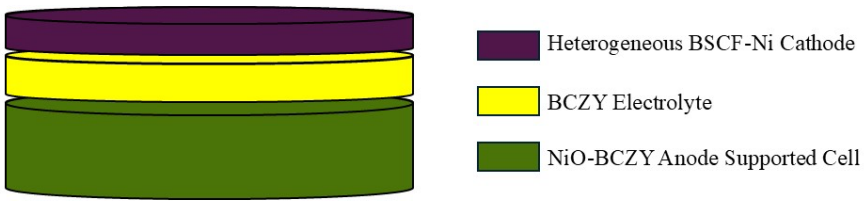

Figure 1. Schematic configuration of an anode-supported single cell

Characterization

The electrochemical performance of the cell was tested using an in-house-developed SOFC testing station, interfaced with a ZIVE SP2 Electrochemical Workstation (ZIVE LAB WonATech) with a perturbation amplitude of 10 mV over a frequency range of 10 mHz-1 MHz, using Pt as the current collector. The cell was subjected to temperature 750 °C, with the anode exposed to 10% H_2 + 90% N_2 as the fuel and stagnant air serving as the oxidant on the cathode side. The fitting procedure was performed using an equivalent circuit model (ECM) and analyzed via complex nonlinear least-squares (CNLS) using Zman software.

The impedance data is further analyzed using distribution relaxation time (DRT) to extract the chemical reactions occurring during the cell's operation by using DRT tools in Matlab software. The peak position and peak area in DRT profiles can reflect the types of chemical processes and their corresponding values. The polarization resistance (R_p) value from DRT is equal to the area under the peak. The regularization parameter was carefully selected to achieve an optimal balance between accuracy and noise suppression in the DRT calculation. A first-order regularization derivative and a Gaussian method for discretization were applied using the DRTtools software.

RESULTS AND DISCUSSION

The morphological study of the heterostructure BSCF-Ni is shown in Figure 2. It reveals the presence of fine nanospheres shape around the nanotube structure. The coexistence of these two structures indicates the successful formation of the intended heterogeneous morphology. The porous nanotube network is expected to enhance gas diffusion, while the nanoparticles provide additional active reaction sites.

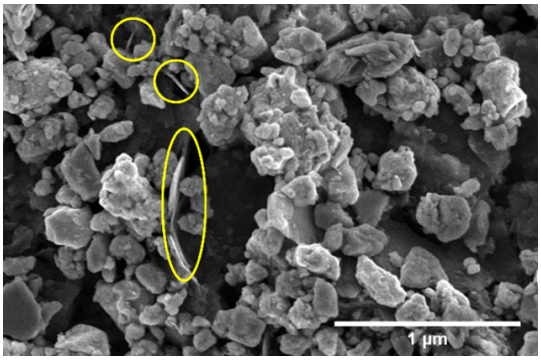

Figure 2. SEM images of the heterogeneous BSCF-Ni (yellow circle: nanotube structure)

Figure 3 shows the electrochemical impedance spectra of the single cell for heterogeneous BSCF-Ni and homogeneous BSCF-Ni in the form of a Nyquist plot at a temperature 750 °C. The spectra exhibit depressed semicircles, indicating non-ideal capacitive behavior, a phenomenon commonly associated with distributed electrochemical processes at electrode–electrolyte interfaces. The impedance response can be qualitatively divided into three overlapping contributions: i) a high-frequency arc attributed to bulk ionic transport and contact resistance; ii) a mid-frequency arc associated

with charge-transfer processes at the electrode surface, and iii) a low-frequency arc related to gas diffusion and surface adsorption [18,19].

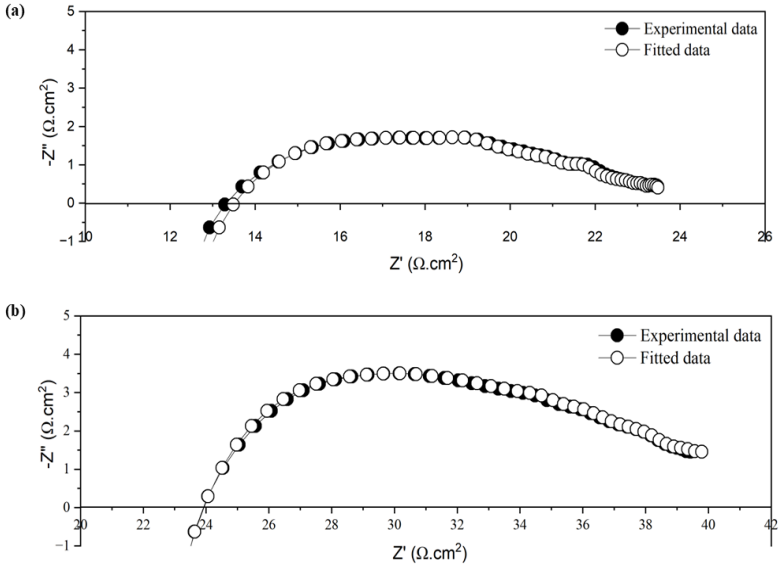

Figure 3. Impedance spectrum of the single cell for (a) Heterogeneous BSCF-Ni (b) Homogeneous BSCF-Ni

The impedance data that was analyzed using CNLS contains five impedance elements with a combination in series of inductor (L_s), distributed elements resistance (R) and constant phase elements (Q) connected in parallel, which is L_sR_s (R_1Q_1) (R_2Q_2) (R_3Q_3) (R_4Q_4) (R_5Q_5) [20]. Although CNLS fitting captures the overall impedance trend (ohmic and polarization resistances) as listed in Table 1, the strong overlap between arcs introduces uncertainty in the physical assignment of individual circuit elements. In systems where microstructural heterogeneity is reduced, and electrochemical processes occur on similar timescales, the impedance response tends to merge individual relaxations into a composite feature rather than distinct, isolated peaks. Overlap can result when charge transfer, mass transport, and surface exchange steps are tightly coupled, or when the physical pathways for these processes (e.g., electronic and ionic conduction networks) are highly interconnected, resulting in a distribution of relaxation times that smears individual contributions into overlapping signals [21].

To elucidate the underlying reaction mechanisms and to decouple the electrochemical responses originating from the cathode and anode, the impedance spectra were further analyzed using the Distribution of Relaxation Times (DRT), as shown in Figure 4. In a heterogeneous structure (Figure 4(a)), different phases (mixed ionic-electronic conducting BSCF, metallic Ni particles, grain boundaries, and triple-phase boundary regions) contribute unique resistive and capacitive elements with disparate kinetics, leading to resolvable peaks each attributable to a particular physical process [21,22]. By contrast, the homogeneous BSCF-Ni sample (Figure 4(b)) shows overlapping peaks that are broader and less well separated along the frequency axis, reflecting a more uniform microstructure and closely spaced time constants for the contributing processes [21].

Table 1. Ohmic resistance (R_o) and polarization resistance (R_p) extracted from CNLS

Sample	Ohmic resistance (R_O), Ω.cm^2	Polarization resistance (R_P), Ω.cm^2					
		R_1	R_2	R_3	R_4	R_5	Total R_P
Heterogeneous BSCF-Ni	13.27	5.45	2.07	1.32	1.02	0.34	10.20
Homogeneous BSCF-Ni	23.84	9.21	2.39	2.05	1.25	0.47	15.37

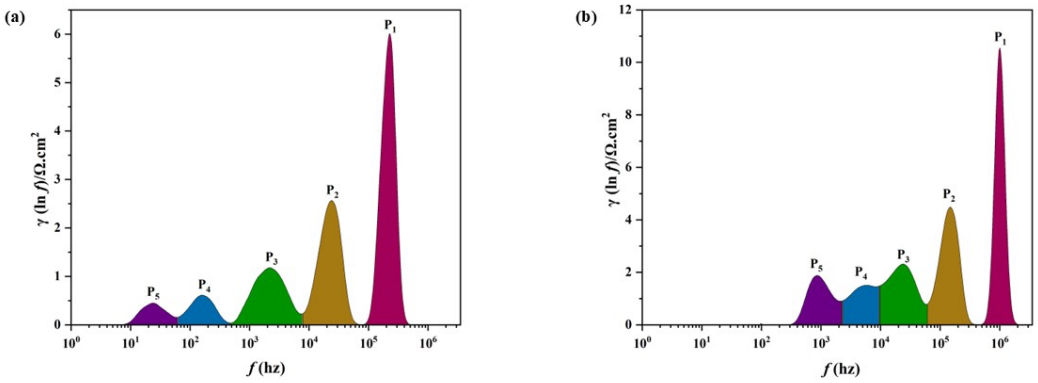

Figure 4. DRT plot for a) heterogeneous BSCF-Ni and b) homogeneous BSCF-Ni with sub-process at different frequency regions

Table 2. Ohmic resistance (R_o) and polarization resistance (R_p) extracted from DRT

Sample	Ohmic resistance (R_O), Ω.cm^2	Polarization resistance (R_P), Ω.cm^2					
		R_1	R_2	R_3	R_4	R_5	Total R_P
Heterogeneous BSCF-Ni	13.27	6.00	2.56	1.17	0.62	0.45	10.80
Homogeneous BSCF-Ni	23.84	11.14	4.49	2.31	1.51	1.87	21.32

The comparable ohmic resistance (R_o) values obtained from both DRT (Table 2) and CNLS (Table 1) analyses indicate that R_o is primarily governed by bulk electrolyte and contact resistances, which are accurately determined from the high-frequency intercept of the impedance spectrum and are largely independent of the analysis method [14]. In contrast, the polarization resistance (R_p) derived from DRT is consistently higher than that obtained from CNLS fitting, particularly for the homogeneous BSCF-Ni cathode, because CNLS relies on predefined equivalent circuit models that can oversimplify complex electrode behavior by merging or underestimating overlapping electrochemical processes with similar time constants [23,24,25]. DRT analysis provides a model-free deconvolution of the impedance response, enabling clearer resolution of multiple relaxation processes (P_1–P_5) associated with charge transfer, oxygen surface exchange, solid-state diffusion, and mass transport, which are often masked in CNLS analysis [14,26]. As a result, DRT captures additional resistive contributions from electrode

kinetics and transport limitations, making it more sensitive to microstructural differences between heterogeneous and homogeneous BSCF-Ni electrodes and providing a more physically representative interpretation of their electrochemical behavior.

The DRT analysis clearly resolves five relaxation processes (P1–P5), which are consistently observed in both heterogeneous BSCF-Ni and homogeneous BSCF-Ni, as commonly observed in well-defined SOFC electrodes [27,28]. In both configurations, the high-frequency peak P_1 (10^5–10^6 Hz) is attributed to charge transfer across the electrolyte cathode interface; however, its lower magnitude in the heterogeneous cathode indicates reduced interfacial resistance and improved electronic percolation arising from spatially optimized Ni and BSCF domains [29,30,31]. The intermediate-frequency peaks P_2 and P_3 (10^3–10^5 Hz), associated with oxygen surface exchange and near-surface oxygen diffusion, are better resolved and less intense in the heterogeneous structure, suggesting accelerated ORR kinetics and weakened kinetic coupling due to hierarchical nanotube–nanosphere morphology [30,32,33]. In contrast, the homogeneous cathode exhibits broadened and overlapping P_2–P_4 features, indicating convergence of surface exchange, adsorption, and diffusion time constants, a hallmark of microstructurally constrained mixed ionic and electronic conducting cathode (MIEC) cathodes [29,34]. Furthermore, the reduced low-frequency contribution (P_5) in the heterogeneous electrode confirms enhanced gas transport enabled by interconnected porosity, whereas the homogeneous structure displays a stronger gas-diffusion-related response [29,30,34]. The DRT peak denotation and mechanism interpretation are tabulated in Table 3.

Table 3. DRT peak denotation and mechanism interpretation

Peak	Frequency range (Hz)	Dominant process	Heterogeneous BSCF-Ni	Homogeneous BSCF-Ni
P_1	10^5–10^6	Charge transfer at the electrolyte–cathode interface	Sharp, lower intensity → fast interfacial kinetics and good electronic pathways	Higher intensity → localized electronic bottlenecks
P_2	10^4–10^5	Oxygen incorporation/ surface exchange	Reduced magnitude → enhanced ORR activity and abundant active sites	Stronger, broader → slower surface exchange
P_3	10^3–10^4	Near-surface oxygen diffusion	Well-resolved → shortened diffusion length via hierarchical morphology	Overlapping with P_2/P_4 → coupled kinetics
P_4	~10^2–10^3	Oxygen adsorption/desorption	Small contribution → efficient gas–solid interaction	Noticeable peak → limited adsorption dynamics
P_5	≤10^2	Gas-phase diffusion/pore transport	Minimal → good pore connectivity	Larger → gas transport limitation

CONCLUSIONS

In conclusion, Ni-doping and tailoring the homogeneous BSCF structure into a heterogeneous structure in the cathode result in lower resistance at T=750 ºC. This indicates that the Ni doping and structural tailoring function well as an oxygen reduction electrode by enabling oxygen vacancy formation, along with fast oxygen incorporation and diffusion kinetics, thereby enabling superior electrochemical activity for ORR. The lowest R_p of the cell obtained is 10.80 Ω cm^2 for the heterogeneous BSCF-Ni cathode. Although this polarization resistance remains higher than that reported in previous study, the present study provides valuable insight into the influence of Ni incorporation and heterogeneous nanostructuring on cathodic reaction mechanisms. Furthermore, DRT has demonstrated its ability to differentiate between anode and cathode processes, providing a deeper understanding of the cell's electrochemical behavior. The indispensable role of DRT as a complement to CNLS is highlighted by these advancements, paving the way for further progress in PCFC technology.

ACKNOWLEDGEMENTS

This work was supported by the Malaysian Toray Science Foundation (MTSF) and Strategic Research Partnership (SRP) Grant (100-RMC 5/3/SRP (084/2021).

REFERENCES

[1] Sumi H, Shimada H, Yamaguchi Y, Mizutani Y, Okuyama Y, Amezawa K. Comparison of electrochemical impedance spectra for electrolyte-supported solid oxide fuel cells (SOFCs) and protonic ceramic fuel cells (PCFCs). *Scientific Reports*. 2021;11(1):10622.

[2] Zeng Q, Zhang X, Wang W, Zhang D, Jiang Y, Zhou X, et al. A Zn-doped $Ba_{0.5}Sr_{0.5}Co_{0.8}Fe_{0.2}O_{3-\delta}$ perovskite cathode with enhanced ORR catalytic activity for SOFCs. *Catalysts*. 2020;10(2):235.

[3] Qiu P, Li J, Jia L, Chi B, Pu J, Li J, et al. $LaCoO_{3-\delta}$ coated $Ba_{0.5}Sr_{0.5}Co_{0.8}Fe_{0.2}O_{3-\delta}$ cathode for intermediate temperature solid oxide fuel cells. *Electrochimica Acta*. 2019;319:981-989.

[4] Zhu W, Lü Z, Wang L, Guan X, Zhang X. Performance of $Ba_{0.5}Sr_{0.5}Co_{0.8}Fe_{0.2}O_{3-\delta}$-Ag composite. *Advanced Materials Research.* 2011;311:2309-2314

[5] Lee S, Lim Y, Lee EA, Hwang HJ, Moon J-W. $Ba_{0.5}Sr_{0.5}Co_{0.8}Fe_{0.2}O_{3-\delta}$ (BSCF) and $La_{0.6}Ba_{0.4}Co_{0.2}Fe_{0.8}O_{3-\delta}$ (LBCF) cathodes prepared by combined citrate-EDTA method for IT-SOFCs. *Journal of Power Sources*. 2006;157(2):848-854.

[6] Yan A, Cheng M, Dong Y, Yang W, Maragou V, Song S, et al. Investigation of a $Ba_{0.5}Sr_{0.5}Co_{0.8}Fe_{0.2}O_{3-\delta}$ based cathode IT-SOFC: I. The effect of CO_2 on the cell performance. *Applied Catalysis B: Environmental.* 2006;66(1-2):64-71.

[7] Li L, Yang H, Gao Z, Zhang Y, Dong F, Yang G, et al. Nickel-substituted $Ba_{0.5}Sr_{0.5}Co_{0.8}Fe_{0.2}O_{3-\delta}$: a highly active perovskite oxygen electrode for reduced-temperature solid oxide fuel cells. *Journal of Materials Chemistry A.* 2019;7(19):12343-12349.

[8] Habiballah AS, Osman N, Jani AMM. Microstructural investigation of BSCF-based cathode material for enhanced oxygen reduction reaction performance and electrode stability. *Ceramics International.* 2020;46(14):23262-23265.
[9] Habiballah AS, Jani AMM, Mahmud AH, Osman N, Radiman S. Facile synthesis of $Ba_{0.5}Sr_{0.5}Co_{0.8}Fe_{0.2}O_{3-\delta}$ (BSCF) perovskite nanowires by templating from nanoporous anodic aluminium oxide membranes. *Materials Chemistry and Physics*. 2016;177:371-388.
[10] Safian SD, Abd Malek NI, Malik LA, Azad AK, Luengchavanon M, Tseng CJ, et al. Lanthanum-Ferrite based cathode: Impedance data interpretation via complex nonlinear least-squares and distribution of relaxation times analyses. *Ceramics International.* 2024;50(20):40518-405125.
[11] Malik LA, Samat AA, Jani AMM, Jamil Z, Othman NH, Tseng C-J, et al. Electrode reaction routes analyses of modified Ni-BCZY anode via distribution relaxation times: 1-D interpretation. *Materials Chemistry and Physics*. 2025;333:130353.
[12] Plank C, Bergmann TG, Schlüter N, Danzer MA. Distribution of Relaxation Times Analysis for Impedance Spectra Containing Resistive-Inductive Characteristics: Part I. Deconvolution Methods. *Journal of the Electrochemical Society.* 2025;172(6):060514.
[13] Piccioni A, Vecchi P, Vecchi L, Grandi S, Caramori S, Mazzaro R, et al. Distribution of relaxation times based on lasso regression: a tool for high-resolution analysis of IMPS data in photoelectrochemical systems. *The Journal of Physical Chemistry C*. 2023;127(17):7957-7964.
[14] Ciucci F, Chen C. Analysis of electrochemical impedance spectroscopy data using the distribution of relaxation times: A Bayesian and hierarchical Bayesian approach. *Electrochimica Acta*. 2015;167:439-454.
[15] Li X, Ahmadi M, Collins L, Kalinin SV. Deconvolving distribution of relaxation times, resistances and inductance from electrochemical impedance spectroscopy via statistical model selection: Exploiting structural-sparsity regularization and data-driven parameter tuning. *Electrochimica Acta.* 2019;313:570-583.
[16] Abdullah NA, Hasan S, Osman N. Role of CA‐EDTA on the Synthesizing Process of Cerate‐Zirconate Ceramics Electrolyte. *Journal of Chemistry*. 2013;2013(1):908340.
[17] Senari SM, Osman N, Jani AM. Impedance Study on NiO-BaCe0. 54Zr0. 36Y0. 1O2. 95 Composite Anode for Proton-Conducting Fuel Cell. *Journal of Physics: Conference Series* 2026;1083(1):012026.
[18] Barsukov Y, Macdonald JR. Electrochemical impedance spectroscopy. *Characterization of Materials*. 2012;2:898-913.
[19] Klotz D, Leonide A, Weber A, Ivers-Tiffée E. Electrochemical model for SOFC and SOEC mode predicting performance and efficiency. *International Journal of Hydrogen Energy.* 2014;39(35):20844-20849.
[20] Shi N, Su F, Huan D, Xie Y, Lin J, Tan W, et al. Performance and DRT analysis of P-SOFCs fabricated using new phase inversion combined tape casting technology. *Journal of Materials Chemistry A*. 2017;5(37):19664-19671.
[21] Wang Z. Distribution of relaxation times for impedance analysis in batteries and fuel cells. *Nature Reviews Clean Technology*. 2025:1;453.

[22] Song X, Wang C, Xu N, Xu Z, Meng J. Performance optimization of metal-supported solid oxide fuel cells using cathode and full cell impregnation with $La_{0.4}Sr_{0.6}Co_{0.2}Fe_{0.7}Nb_{0.1}O_{3-\delta}$ electrode. *RSC Advances.* 2024;14(41):30460-20468.
[23] Wagner N, Schnurnberger W, Müller B, Lang M. Electrochemical impedance spectra of solid-oxide fuel cells and polymer membrane fuel cells. *Electrochimica Acta*. 1998;43(24):3785-3793.
[24] Das D, Lvov SN. Subtraction impedance spectra in solid oxide fuel cells operating on alternative fuel reformate streams poisoned by inorganic impurities. *ECS Meet Abstr.* 2016;MA2016-01:1410.
[25] Leonide A, Apel Y, Ivers-Tiffee E. SOFC modeling and parameter identification by means of impedance spectroscopy. *ECS Transactions.* 2009;19(20):81.
[26] Boukamp BA, Rolle A. Use of a distribution function of relaxation times (DFRT) in impedance analysis of SOFC electrodes. *Solid State Ionics*. 2018;314:103-111.
[27] Boukamp BA. A linear Kronig‐Kramers transform test for immittance data validation. *Journal of the Electrochemical Society.* 1995;142(6):1885.
[28] Adler SB. Factors governing oxygen reduction in solid oxide fuel cell cathodes. *Chemical Reviews*. 2004;104(10):4791-4844.
[29] Cui T, Li H, Lyu Z, Wang Y, Han M, Sun Z, et al. Identification of electrode process in large-size solid oxide fuel cell. *Acta Phys Chim Sin*. 2020;38:2011009.
[30] Wang X, Lu Y, Xie C, Wang Y, Li H, Ding X. Hetero-structured composite cathodes by electrospinning with high CO_2-poisoning tolerance for solid oxide fuel cells. *International Journal of Hydrogen Energy.* 2024;50:1137-1146.
[31] Nielsen J, Hjelm J. Impedance of SOFC electrodes: A review and a comprehensive case study on the impedance of LSM: YSZ cathodes. *Electrochimica Acta.* 2014;115:31-45.
[32] Zhou W, Liang F, Shao Z, Chen J, Zhu Z. Heterostructured electrode with concentration gradient shell for highly efficient oxygen reduction at low temperature. *Scientific Reports*. 2011;1(1):155.
[33] Xia B, Zhang H, Yao C, Lou H, Chen M, Zhang Z, et al. Enhancing ORR activity and CO_2 tolerance of $Pr_{0.4}Sr_{0.6}Co_{0.2}Fe_{0.8}O_{3-\delta}$-based SOFC cathode through synergistic doping and surface modification. *Applied Surface Science*. 2024;649:159143.
[34] Chen X, Yu N, Bello IT, Zhang D, Zhou J, Wang Y, et al. Understanding the oxygen reduction reaction in the hierarchically oriented composite cathode with open, straight pores. *Separation and Purification Technology*. 2023;325:124713.